Graphene-based terahertz tunable plasmonic directional coupler

Meng-Dong He, Kai-Jun Wang, Lei Wang, Jian-Bo Li, Jian-Qiang Liu, Zhen-Rong Huang, Lingling Wang, Lin Wang, Wei-Da Hu, and Xiaoshuang Chen

Citation: Applied Physics Letters **105**, 081903 (2014); doi: 10.1063/1.4894090
View online: http://dx.doi.org/10.1063/1.4894090
View Table of Contents: http://scitation.aip.org/content/aip/journal/apl/105/8?ver=pdfcov
Published by the AIP Publishing

Graphene-based terahertz tunable plasmonic directional coupler

Meng-Dong He,[1,a)] Kai-Jun Wang,[1] Lei Wang,[1] Jian-Bo Li,[1] Jian-Qiang Liu,[2] Zhen-Rong Huang,[3] Lingling Wang,[3] Lin Wang,[4] Wei-Da Hu,[4] and Xiaoshuang Chen[4]
[1]*Institute of Mathematics and Physics, Central South University of Forestry and Technology, Changsha 410004, People's Republic of China*
[2]*College of Science, Jiujiang University, Jiujiang 332005, People's Republic of China*
[3]*Key Laboratory for Micro-Nano Optoelectronic Devices of Ministry of Education, Hunan University, Changsha 410082, People's Republic of China*
[4]*National Laboratory for Infrared Physics, Shanghai Institute of Technical Physics, Chinese Academy of Science, Shanghai 200083, People's Republic of China*

(Received 12 May 2014; accepted 15 August 2014; published online 26 August 2014)

We propose and numerically analyze a terahertz tunable plasmonic directional coupler which is composed of a thin metal film with a nanoscale slit, dielectric grating, a graphene sheet, and a dielectric substrate. The slit is employed to generate surface plasmon polaritons (SPPs), and the metal-dielectric grating-graphene-dielectric constructs a Bragg reflector, whose bandgap can be tuned over a wide frequency range by a small change in the Fermi energy level of graphene. As a graphene-based Bragg reflector is formed on one side of the slit, the structure enables SPP waves to be unidirectionally excited on the other side of the slit due to SPP interference, and the SPP waves in the Bragg reflector can be efficiently switched on and off by tuning the graphene's Fermi energy level. By introducing two optimized graphene-based Bragg reflectors into opposite sides of the slit, SPP waves can be guided to different Bragg reflectors at different Fermi energy levels, thus achieving a tunable bidirectional coupler. © *2014 AIP Publishing LLC*.
[http://dx.doi.org/10.1063/1.4894090]

In the past decade, manipulating and controlling the intensity and propagation direction of surface plasmon polaritons (SPPs) in plasmonic structures has been a research hotspot in the fields of plasmonics, metal optics, and optical metamaterials,[1–3] since it is vital and essential to the realization of many nanoscale optical devices including waveguides, couplers, splitters, modulators, switches, etc. Taking SPP waves excited by a metallic nanoslit as an example. Several control schemes have been proposed that make SPP waves propagate along a desired direction. One scheme is to employ the ability for confining SPPs of grating structures. By placing two optimized grating structures on opposite sides of the slit, the SPP waves at different frequencies can be guided in the two predetermined directions.[4–6] Another scheme is based on SPP interference. By modulating the relative phase difference between two SPP waves, the electromagnetic field intensity along one direction on the metal surface can be enhanced (or suppressed) due to the constructive (or destructive) interference of SPPs, thus the propagation direction of SPP wave is under control.[7–10] In addition, SPP directional propagation can also be achieved in a partial dielectric filled slit structure by SPP wavevector matching.[11]

Even though the above schemes effectively manipulate the propagation direction of SPP waves in a metallic slit structure, the SPP waves cannot be actively controlled. The ability to actively control SPP waves in a metallic slit will enable dynamic tuning of SPP waves and will potentially expand the range of their applications even further. In addition, the above studies of SPPs mainly focus on the visible and infrared frequency range due to the poor confinement of SPPs at low frequencies, such as terahertz (THz) frequency. Actually SPPs at THz frequency have a broad range of potential applications.[12,13] In recent years, graphene, a single layer of carbon atoms arranged in a honeycomb lattice, has been demonstrated to support well-confined SPPs at THz frequency since the imaginary part of its complex conductivity is positive.[14–16] Graphene plasmons provide a suitable alternative to noble metal plasmons due to their tighter confinement and longer lifetime.[17,18] More importantly, graphene plasmons can be dynamically tuned by electrochemical potential via chemical or electrostatic gating, magnetic field, or optical excitation.[19,20] Just because of the unique property, graphene enables active control or dynamic tuning of SPP modes in many plasmonic structures.[21–26] Inspired by the finding, we think that it is possible that the SPP modes generated by a metallic slit are effectively turned on and off or directionally coupled by using the tunability of graphene. In this paper, we propose a plasmonic structure, in which dielectric gratings are sandwiched between a single nanoscale metallic slit and a graphene sheet on top of a dielectric substrate. The structure not only can highly confine and guide THz SPP modes in the dielectric gratings, but also has the ability to tune SPP wave propagation direction, which can be used to build a tunable plasmonic coupler and can, therefore, open an avenue for active photonic integrated circuits.

Fig. 1 depicts the schematic of our proposed structure, where two SiO_2 gratings are sandwiched between a silver (Ag) film with a nanoscale slit and a graphene sheet on the top of SiO_2/p^+Si substrate. A plane wave of TM polarization (the magnetic field is perpendicular to the x– z plane) impinges normally on the top of the structure. The geometry

[a)]Author to whom correspondence should be addressed. Electronic mail: hemendong@sohu.com

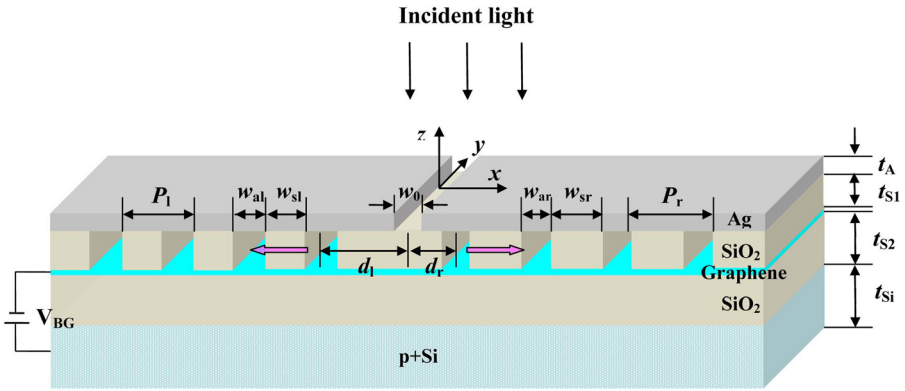

FIG. 1. Schematic of our proposed structure, which is composed of a thin silver (Ag) film with a nanoscale slit, two SiO_2 gratings, a graphene sheet and SiO_2/p^+Si substrate. w_0 is the width of metallic slit; t_A, t_{S1}, t_{S2}, and t_{Si} denote the thicknesses of Ag film, SiO_2 gratings, SiO_2 dielectric layer, and p^+Si substrate, respectively. $P_{r(l)}$, $w_{ar(al)}$, and $w_{sr(sl)}$ are the period, the widths of air and SiO_2 layers of the right (left) dielectric grating, respectively, and $d_{r(l)}$ stands for the separation between the slit and the first air-trench of the right (left) grating (defined centre to centre).

is defined by following parameters. w_0 denotes the width of metallic slit, $t_{A(S1,S2,Si)}$ is the thickness of Ag film (SiO_2 gratings, SiO_2 dielectric layer, p^+Si substrate), $P_{r(l)}$, $w_{ar(al)}$, and $w_{sr(sl)}$ represent the period, the widths of air and SiO_2 layers of the right (left) dielectric grating, respectively, and $d_{r(l)}$ stands for the separation between the slit and the first air-trench of the right (left) grating (defined centre to centre). The graphene sheet may be modeled as an anisotropic dielectric constant expressed by a diagonal tensor.[27] Its surface-normal component is set as $\varepsilon_{zz} = 2.5$ based on the dielectric constant of graphite, and its in-plane component is expressed by $\varepsilon_{xx(yy)} = 2.5 + i\sigma_g/(\varepsilon_0 \omega t)$, where σ_g and t (0.5 nm) are the frequency dependence of surface conductivity and the thickness of graphene sheet, respectively. At THz frequencies, σ_g can be described by a Drude-like expression $\sigma_g = i(e^2 E_f/\pi\hbar^2)/(\omega + i\tau^{-1})$,[27,28] where E_f and τ represent the Fermi energy level and the carrier relaxation time of graphene, respectively. E_f and τ are given by $\hbar v_f (\pi n)^{1/2}$ and $\mu E_f / e v_f^2$, respectively,[27] where n, v_f (10^6 m/s), and μ (10 000 cm^2/Vs (Ref. 29)) stand for the carrier concentration, Fermi velocity, and carrier mobility of graphene, respectively. The permittivities of SiO_2 and p^+Si are taken to be 3.9 and 11.9, respectively, and the metal silver is modeled as a perfect electric conductor for the THz frequency range of interest. To allow for doping through electrostatic gating, p^+Si is employed as a back-gate. By applying a voltage between the graphene sheet and the back-gated p^+Si, the carrier concentration and thus the Fermi energy level of graphene can be electrically tuned,[23,24,30] which will be used to control graphene plasmon wave subsequently. In this paper, the numerical calculations for field distribution and transmission spectrum are performed by using Lumerical FDTD solutions based on the finite-difference time-domain method.

First, we analyze the dispersion characteristics of a insulator-graphene-insulator-metal (IGIM) waveguide. For a SPP mode with propagation constant β in a IGIM waveguide, its dispersion equation is expressed by[31]

$$\frac{-\gamma_1 \varepsilon_2}{\gamma_2 \varepsilon_1} = \left(1 + \frac{i\sigma_g \gamma_1}{\omega \varepsilon_1}\right) \tanh(\gamma_2 t), \tag{1}$$

where t denotes the thickness of the inner insulator between graphene sheet and metal film, ε_1 and ε_2 are the permittivities of the outer and inner insulators, respectively, $\gamma_1 = \sqrt{\beta^2 - \varepsilon_1 k_0^2/\varepsilon_0}$ and $\gamma_2 = \sqrt{\beta^2 - \varepsilon_2 k_0^2/\varepsilon_0}$ represent the attenuation constants in the outer and inner insulators, respectively, and k_0 is the wavenumber in free space. β is obtained by solving the above transcendental equation, and then the effective index of SPP mode is given by $n_{eff} = \beta/k_0$. In this paper, SiO_2 is used as the outer insulator, and its thickness is set as 400 nm. Since the thickness is much larger than the decay length of SPP over the dielectric medium SiO_2, Eq. (1) is valid for the above case. Taking $t = 40$ nm, we calculate the dispersion of the mode index n_{eff} for two inner insulators (air and SiO_2) and two values of E_f (0.3 and 0.6 eV). The real part of n_{eff} (i.e., real(n_{eff})) is plot in Fig. 2(a). As shown in previous works,[31] with the increase of frequency real(n_{eff}) initially drops quickly and then increases gradually after reaching a minimum. For a given insulator and a given frequency, a

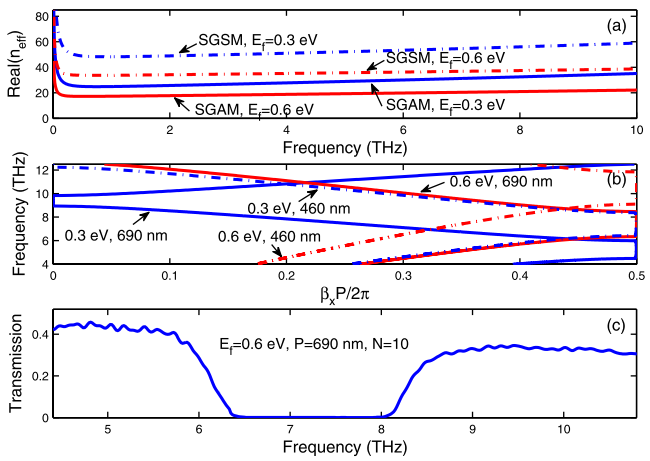

FIG. 2. (a) Real parts of the effective refractive indexs of SPP modes in SGAM waveguide and SGSM waveguide as a function of frequency for different Fermi energy levels. (b) Dispersion curves of SPP modes in Bragg reflector for different values of E_f and P. The widths of air and SiO_2 layers in the Bragg reflector with $P = 690$ (460) nm are 340 (230) and 350 (230) nm, respectively, and both the thicknesses of air and SiO_2 layers are 40 nm. The two numbers in each group of numbers in figure present the Fermi energy level and the period of dielectric grating, respectively. (c) Transmission spectrum of the Bragg reflector with $E_f = 0.6$ eV, $P = 690$ nm, and period of Bragg cell $N = 10$.

lower Fermi energy level corresponds to a larger real(n_{eff}). For the same Fermi energy level and the same frequency, real(n_{eff}) for SiO_2 is much greater than that for air, meaning that SPP mode in SiO_2-graphene-SiO_2-metal (SGSM) waveguide is tighter than that in SiO_2-graphene-air-metal (SGAM) waveguide.

As the SGSM and SGAM waveguides are alternatively stacked, a graphene-based plasmonic Bragg reflector is formed, whose formation is different from that of the plasmonic Bragg reflector in recent works.[32] The dispersion relation of SPP mode along the x direction can be calculated by incorporating effective index into the secular equation[33]

$$\cos(\beta_x P) = \cos(\beta_a w_a)\cos(\beta_s w_s) - \frac{1}{2}\left(\frac{n_{effs}}{n_{effa}} + \frac{n_{effa}}{n_{effs}}\right)\sin(\beta_a w_a)\sin(\beta_s w_s), \quad (2)$$

where β_x denotes the propagation constant of SPP mode along the x direction, w_a and w_s are the widths of air and SiO_2 layers, respectively, P is the period of Bragg reflector ($P = w_a + w_s$), and $\beta_{a(s)}$ and $n_{effa(s)}$ correspond to the propagation constant and effective index of SPP mode in SGAM (SGSM) waveguide, respectively. Figure 2(b) displays the dispersion curves of SPP modes for different values of E_f and P. For the Bragg reflector of $P = 690$ nm ($w_a = 340$ and $w_s = 350$ nm), at $E_f = 0.3$ eV, the dispersion curve has a bandgap located at the frequency range of [4.50, 5.98] THz. When E_f increases to 0.6 eV, the bandgap exhibits a large blue shift ([6.34, 8.47] THz). It suggests that a small change of Fermi energy level leads to a broad tuning range of the bandgap. With respect to the Bragg reflector with $P = 460$ nm ($w_a = 230$ and $w_s = 230$ nm), its bandgap changes from [6.44, 8.37] THz to [9.10, 11.84] THz as E_f increases from 0.3 to 0.6 eV. According to the Bragg condition $w_a\text{real}(n_{effa}) + w_s\text{real}(n_{effs}) = m\lambda_b/2$ (m is an integer),[32] we can obtain the Bragg wavelength λ_b. For the Bragg reflector with $P = 690$ nm and $E_f = 0.6$ eV, the calculated Bragg wavelength is about 40 μm (corresponding to $m = 1$), and its corresponding Bragg frequency (7.5 THz) is just localized in the bandgap of [6.34, 8.47] THz, confirming the validity of Eqs. (1) and (2). Using Lumerical FDTD solutions, we also calcualted the transmission spectrum of Bragg reflector with $P = 690$ nm, $E_f = 0.6$ eV, and period of Bragg cell $N = 10$, as shown in Fig. 2(c). One can see that there is a wide stopband with near-zero transmission around the Bragg frequency of 7.5 THz, which shows a good filtering characteristic and is in good agreement with the corresponding dispersion curve in Fig. 2(b).

If the above Bragg reflector with $P = 690$ nm and $E_f = 0.6$ eV is only formed on the right-side output surface of the illuminated slit (as shown in the inset in Fig. 3(a)), SPP modes are excited by the slit, and at the Bragg frequency, constructive SPP interference would occur on the left-side surface as the condition of phase matching is satisfied,[7] suggesting that the device would behave as an efficient source for unidirectional SPPs. To verify this analysis, we calculated the electric field distribution of $|E_z|$ at the Bragg frequency (7.5 THz), as shown in Fig. 3(a). It is clear that the electric field is highly confined in the space between the metal film and the graphene sheet due to the large real(n_{eff})

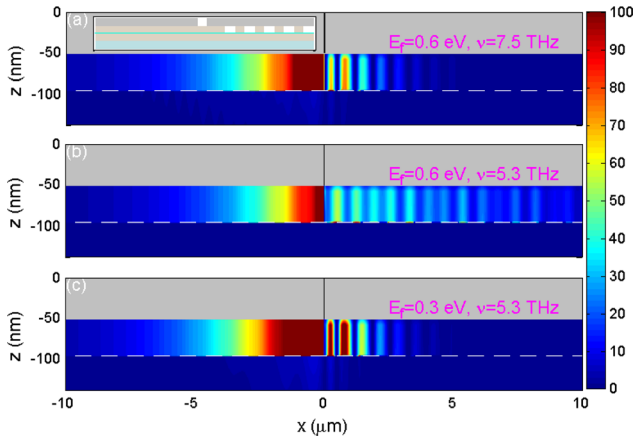

FIG. 3. Electric field profiles of $|E_z|$ in the plasmonic coupler based on the graphene Bragg reflector with $E_f = 0.6$ eV and $\nu = 7.5$ THz (a), $E_f = 0.6$ eV, and $\nu = 5.3$ THz (b), and $E_f = 0.3$ eV and $\nu = 5.3$ THz (c). The inset in (a) shows the schematic of the plasmonic coupler. The geometry parameters of the graphene Bragg reflector are the same as those of the Bragg reflector with $P = 690$ nm in Fig. 2(b). The thicknesses of SiO_2 grating (t_{S1}), metal film (t_A), SiO_2 layer (t_{S2}), and p^+Si substrate (t_{Si}) are 40, 50, 400, and 500 nm, respectively, and the width of the metallic slit (w_0) is 40 nm. The incident plane wave with a unitary electric field is incident normally from the top of the structure. The gray areas and white dashed lines denote the metal and the graphene sheet, respectively.

of SPP mode. The steady-state optical intensity within the region $x > 1.4$ μm is very weak because of the reflection effect of Bragg reflector. The constructive interference of the reflected SPP with the one leaving the slit occurs on the left-side output surface, thus most of energy propagates along the negative direction of the x axis. As emphasized in Ref. 7, the SPP interference effect is sensitive to the separation between the slit and the first air trench, so we should choose a suitable separation for SPP directional coupling. For the frequency of 5.3 THz, which is outside of the bandgap of the Bragg reflector with $E_f = 0.6$ eV (Fig. 2(b)), we observe that the SPP wave can propagate in the Bragg reflector (Fig. 3(b)). If the Fermi energy decreases to 0.3 eV (Fig. 3(c)), the SPP wave is blocked again by the Bragg reflector because at this time the frequency is inside the bandgap of the Bragg reflector (Fig. 2(b)). The phenomenon in Figs. 3(b) and 3(c) indicates that the SPP mode can be effectively turned on and off by changing the Fermi energy level of the graphene sheet, and the proposed structure can be regarded as a optical switch.

We note that, as the Fermi energy levels of the Bragg reflectors with $P = 690$ and 460 nm in Fig. 2(c) are set as 0.6 and 0.3 eV, respectively, the dispersion curves of the two Bragg reflectors have almost the same bandgap. If the Fermi energy levels of the two Bragg reflectors change to be 0.3 and 0.6 eV, respectively, their bandgaps don't overlap with the respective previous bandgap. The bandgap features of Bragg reflectors can be used to realize bidirectional coupling for SPP waves. We introduce the two graphene Bragg reflectors into a metallic slit structure (as shown in Fig. 1), and calculated the field profiles of $|E_z|$ at $\nu = 7.5$ THz for different Fermi energy levels (as shown in Fig. 4). As the Fermi energy is 0.3 eV, most of energy is guided towards the right-side Bragg reflector. The peak intensity within the region from 0 to 8 μm is 10 to 210 times that of the incident light, while the steady-state optical intensity on the left-hand side surface is relatively weak ($x < -1.6$ μm). As the Fermi

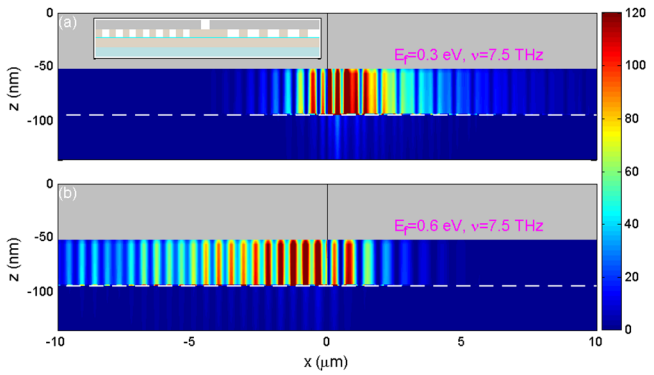

FIG. 4. Electric field profiles of $|E_z|$ in the graphene-based plasmonic coupler for $E_f = 0.3$ eV (a) and $E_f = 0.6$ eV (b). The inset in (a) shows the schematic of the plasmonic coupler. The frequency of the incident light is 7.5 THz. w_{al}, w_{sl}, P_l, d_l, w_{ar}, w_{sr}, P_r, and d_r are taken to be 230, 230, 460, 585, 340, 350, 690, and 880 nm, respectively. The other structural parameters are the same as those in Fig. 3.

energy increases to 0.6 eV, most of the energy propagates towards the left-side Bragg reflector. Simulation results show that the proposed structure is capable of splitting SPPs into two Bragg reflectors, and the direction of SPPs is under active control.

Besides the Fermi energy level of graphene, the THz SPP waves in our proposed structure can also be tuned by changing the geometrical and material parameters (such as the widths, thicknesses and dielectric constants of constituent layers of dielectric grating), since the bandgap position of Bragg reflector is dependent on the parameters. However, it is worth noting that such SPP tuning is passive. Compared to the previous plasmonic directional couplers,[4–11] our graphene-based structure has an appealing advantage: active tunability of SPP waves via electrostatic gating. In addition, the SPP waves in the previous plasmonic directional couplers propagate along the dielectric-metal interface; at THz frequency, they have a large spatial extent in the dielectric medium.[4] While in our structure, the THz SPP modes supported by graphene are confined down to volumes that are far smaller than plasmons in noble metals. At the same time, the THz SPP modes are mainly guided in the space between graphene sheet and metal film. Therefore, the SPP confinement is largely improved in comparison with that in the previous plasmonic directional couplers. Recently, it has been reported that ferroelectric-gated graphene can achieve nanometer order confinement of THz SPPs due to the strong coupling between the plasmons in graphene and the phonon-polaritons in ferroelectrics, at low-THz frequencies the modal wavelength and confining length of surface plasmon-phonon-polaritons are only about 100–200 and 10–20 nm, respectively.[34] In our proposed structure, the modal wavelengths ($2\pi/\mathrm{Re}[\beta_x]$) of SPPs in the right-hand Bragg reflector in Fig. 4(a) and the left-hand Bragg reflector in Fig. 4(b) are about 2.8 and 1.3 μm, respectively. The confining lengths ($1/\mathrm{Re}[\gamma_1]$) of SPPs over the outer insulator SiO_2 in Figs. 4(a) and 4(b) are about 110–200 and 170–300 nm, respectively. The above data indicate that the SPP confinement in our proposed structure is not high in comparison with that in ferroelectrics-gated graphene. In this paper, we do not discuss the effect of superstrate and filing dielectric in metal slit on the plasmon directional coupling. If a dielectric medium is present on the metal film and in the slit, similar phenomena mentioned above can also be observed. Experimentally, our considered structures can be prepared by the following procedures: a CVD-grown graphene is transferred onto a SiO_2/p^+Si substrate. On the other hand, a Ag film is deposited on a dielectric substrate (such as SiO_2) by atomic layer deposition (ALD), a nanoslit is fabricated in the Ag film by using ion beam lithography, then the Ag film is covered by a SiO_2 layer using ALD, and SiO_2 gratings are formed by electron beam lithography. Finally, the structure of SiO_2 grating-Ag film is turned over and is transferred on top of the graphene sheet.

In summary, we have presented and investigated numerically a terahertz tunable directional plasmonic coupler, where SiO_2 grating on top of a graphene-SiO_2–p^+Si substrate is covered by a Ag film with a nanoscale slit. The metal film-dielectric grating-graphene-dielectric forms a plasmonic Bragg reflector. By introducing a graphene-based Bragg reflector to one side of the output surface of a metallic nanoslit, the SPP waves directionally propagate along the other side of the slit due to SPP constructive interference, so the structure can be used as a unidirectional coupler. The structure has also the function of switching the SPP in Bragg reflector since the Bragg reflector's bandgap can be tuned by changing the Fermi energy level of graphene. As two optimized graphene-based Bragg reflectors are placed on opposite sides of the slit, the SPP waves can be guided to different reflectors by adjusting the Fermi energy level; at this time, the structure is regarded as a bidirectional plasmonic coupler (or splitter). We put forward a scheme of controlling the propagation direction of SPP modes excited by a metallic nanoslit, and our proposed structures have potential applications in building active plasmonic photonic circuits.

The authors acknowledge J. Torley and D. Zhou for critical reading of the manuscript. This work was supported by the National Natural Science Foundation of China (Grant Nos. 11174372 and 11264021), the State Key Program for Basic Research of China (Grant No. 2013CB632705), and the Youth Foundation of Hunan Provincial Education Department, China (Grant No. 11B134).

[1]E. Ozbay, Science **311**, 189 (2006).
[2]P. Nagpal, N. C. Lindquist, S. H. Oh, and D. J. Norris, Science **325**, 594 (2009).
[3]W. Cai and V. Shalaev, *Optical Metamaterials: Fundamentals and Applications* (Springer, New York, 2010).
[4]Q. Gan, Z. Fu, Y. J. Ding, and F. J. Bartoli, Opt. Express **15**, 18050 (2007).
[5]Q. Gan and F. J. Bartoli, Opt. Lett. **35**, 4181 (2010).
[6]Y. J. Zhou, Q. Jiang, and T. J. Cui, Opt. Express **19**, 5260 (2011).
[7]F. López-Tejeira, S. G. Rodrigo, L. Martín-Moreno, F. J. García-Vidal, E. Devaux, T. W. Ebbesen, J. R. Krenn, I. P. Radko, S. I. Bozhevolnyi, M. U. González, J. C. Weeber, and A. Dereux, Nat. Phys. **3**, 324 (2007).
[8]T. Xu, Y. Zhao, D. Gan, C. Wang, C. Du, and X. Luo, Appl. Phys. Lett. **92**, 101501 (2008).
[9]J. Chen, Z. Li, S. Yue, and Q. Gong, Appl. Phys. Lett. **97**, 041113 (2010).
[10]S. B. Choi, D. J. Park, Y. K. Jeong, Y. C. Yun, M. S. Jeong, C. C. Byeon, J. H. Kang, Q. H. Park, and D. S. Kim, Appl. Phys. Lett. **94**, 063115 (2009).
[11]M. D. He, J. Q. Liu, K. J. Wang, X. J. Wang, and Z. Q. Gong, Opt. Commun. **285**, 4588 (2012).

[12]H. T. Chen, H. Lu, A. K. Azad, R. D. Averitt, A. C. Gossard, S. A. Trugman, J. F. O'Hara, and A. J. Taylor, Opt. Express **16**, 7641 (2008).
[13]T. Matsui, A. Agrawal, A. Nahata, and Z. V. Vardeny, Nature **446**, 517 (2007).
[14]A. N. Grigorenko, M. Polini, and K. S. Novoselov, Nat. Photonics **6**, 749 (2012).
[15]A. Yu. Nikitin, F. Guinea, and L. Martin-Moreno, Appl. Phys. Lett. **101**, 151119 (2012).
[16]O. Mitrofanov, W. Yu, R. J. Thompson, Y. Jiang, I. Brener, W. Pan, C. Berger, W. A. de Heer, and Z. Jiang, Appl. Phys. Lett. **103**, 111105 (2013).
[17]F. H. L. Koppens, D. E. Chang, and F. J. García de Abajo, Nano Lett. **11**, 3370 (2011).
[18]J. Christensen, A. Manjavacas, S. Thongrattanasiri, F. H. L. Koppens, and F. J. García de Abajo, ACS Nano **6**, 431 (2012).
[19]D. K. Efetov and P. Kim, Phys. Rev. Lett. **105**, 256805 (2010).
[20]Z. Fei, A. S. Rodin, G. O. Andreev, W. Bao, A. S. McLeod, M. Wagner, L. M. Zhang, Z. Zhao, M. Thiemens, G. Dominguez, M. M. Fogler, A. H. Castro Neto, C. N. Lau, F. Keilmann, and D. N. Basov, Nature **487**, 82 (2012).
[21]L. Ju, B. Geng, J. Horng, C. Girit, M. Martin, Z. Hao, H. A. Bechtel, X. Liang, A. Zettl, Y. R. Shen, and F. Wang, Nat. Nanotechnol. **6**, 630 (2011).
[22]P. Liu, W. Cai, L. Wang, X. Zhang, and J. Xu, Appl. Phys. Lett. **100**, 153111 (2012).
[23]B. Sensale-Rodriguez, R. Yan, S. Rafique, M. Zhu, W. Li, X. Liang, D. Gundlach, V. Protasenko, M. M. Kelly, D. Jena, L. Liu, and H. G. Xing, Nano Lett. **12**, 4518 (2012).
[24]S. H. Lee, M. Choi, T. T. Kim, S. Lee, M. Liu, X. Yin, H. K. Choi, S. S. Lee, C. G. Choi, S. Y. Choi, X. Zhang, and B. Min, Nat. Mater. **11**, 936 (2012).
[25]B. Vasić, M. M. Jakovljević, G. Isić, and R. Gajić, Appl. Phys. Lett. **103**, 011102 (2013).
[26]X. Ren, W. E. I. Sha, and W. C. H. Choy, Opt. Express **21**, 31824 (2013).
[27]W. Gao, J. Shu, C. Qiu, and Q. Xu, ACS Nano **6**, 7806 (2012).
[28]M. Jablan, H. Buljan, and M. Soljačić, Phys. Rev. B **80**, 245435 (2009).
[29]K. S. Novoselov, A. K. Geim, S. V. Morozov, D. Jiang, Y. Zhang, S. V. Dubonos, I. V. Grigorieva, and A. A. Firsov, Science **306**, 666 (2004).
[30]W. Gao, G. Shi, Z. Jin, J. Shu, Q. Zhang, R. Vajtai, P. M. Ajayan, J. Kono, and Q. Xu, Nano Lett. **13**, 3698 (2013).
[31]X. Gu, I. T. Lin, and J. M. Liu, Appl. Phys. Lett. **103**, 071103 (2013).
[32]J. Tao, X. C. Yu, B. Hu, A. Dubrovkin, and Q. J. Wang, Opt. Lett. **39**, 271 (2014).
[33]A. Yariv and P. Yeh, *Optical Waves in Crystals* (Wiley, New York, 1984).
[34]D. Jin, A. Kumar, K. H. Fung, J. Xu, and N. X. Fang, Appl. Phys. Lett. **102**, 201118 (2013).